

Treftz Difference Schemes on Irregular Stencils

Igor Tsukerman e-mail: igor@uakron.edu

Department of Electrical and Computer Engineering, The University of Akron,
OH 44325-3904

The date of receipt and acceptance will be inserted by the editor

Abstract The recently developed Flexible Local Approximation Method (FLAME) produces accurate difference schemes by replacing the usual Taylor expansion with Treftz functions – local solutions of the underlying differential equation. This paper advances and casts in a general form a significant modification of FLAME proposed recently by Pinheiro & Webb: a least-squares fit instead of the exact match of the approximate solution at the stencil nodes. As a consequence of that, FLAME schemes can now be generated on irregular stencils with the number of nodes substantially greater than the number of approximating functions. The accuracy of the method is preserved but its robustness is improved. For demonstration, the paper presents a number of numerical examples in 2D and 3D: electrostatic (magnetostatic) particle interactions, scattering of electromagnetic (acoustic) waves, and wave propagation in a photonic crystal. The examples explore the role of the grid and stencil size, of the number of approximating functions, and of the irregularity of the stencils.

Key words Flexible local approximation, finite difference schemes, Treftz functions, electrostatics, wave propagation, wave scattering, electromagnetic waves, multiparticle problems, long-range interactions, irregular stencils, meshless methods, least squares approximation.

1 Introduction

Traditional finite difference analysis relies primarily on Taylor expansions. These are quite general but are accurate only if the underlying solution has the level of smoothness commensurate with the order of the expansion. In particular, the Taylor approximation breaks down at material interfaces due

to jumps in the solution and/or its derivatives. This leads to the well known “staircase effect” in difference schemes (see a discussion of the algebraic nature of this numerical artifact in [1,2]). Other common situations where the Taylor series, and hence the corresponding classical schemes, are inaccurate include boundary layers and sharp peaks or singularities in the vicinity of sources, edges and corners.

The Flexible Local Approximation MEthod (FLAME) [1,2] replaces the Taylor polynomials with much more accurate “Trefftz” approximations by local solutions of the underlying differential equation. As a result, the approximation accuracy and consequently the consistency error of the scheme can be improved dramatically.

Previously, FLAME relied on the point-matching of the nodal values of the local approximation. To fix the key idea, consider a nine-point (3×3) scheme for the Laplace equation in 2D. The solution is approximated locally as a linear combination of eight Trefftz functions, harmonic polynomials being the most natural choice.¹ With nine nodes and only eight free parameters, the nodal values must be linearly dependent. It is the linear relationship between them that constitutes the FLAME scheme. Details and a large variety of examples can be found in [1,2,4,5,6,7]; the applications include electro- and magnetostatics, wave propagation and scattering, the Poisson-Boltzmann equation in macromolecular and colloidal simulation.

One limitation of the point matching procedure is that it links the number of approximating functions and stencil nodes, as evident from the above example of eight basis functions for the nine-point stencil. This connection between functions and nodes has impeded further progress of the method in two different ways.

First, the most natural choices of the stencil and the basis set have not always been feasible. For instance, consider the standard 3×3 stencil in 2D problems involving cylindrical particles. A natural choice of the basis in such cases is cylindrical harmonics [2,5,7] that include the exponential factors $\exp(im\phi)$, $m = 0, \pm 1, \pm 2, \dots$, where ϕ is the polar angle. Since these harmonics come in pairs $\pm m$ for all m except $m = 0$, the “natural” number of functions in this basis is odd. At the same time, to obtain a FLAME scheme on the nine-point stencil, one must choose eight basis functions, which breaks the natural symmetry: only one index m from the pair $m = \pm 4$ can be taken. This is more of a nuisance than an actual detriment because all harmonics up to order $m = 3$ are still included.

A more serious obstacle is that large stencils (in terms of the number of nodes) require in the established version of FLAME a commensurately large number of basis functions. Unfortunately, expanded basis sets tend to be poorly conditioned. Yet large stencils are highly desirable in some circumstances, in particular for irregular distributions of nodes where small

¹ There are of course other possibilities: e.g. functions $r^m \exp(im\phi)$ ($m = 0, \pm 1, \pm 2, \dots$) in a polar coordinate system (r, ϕ) or Green’s functions of the form $|\mathbf{r} - \mathbf{r}_{\text{src}}|^{-1}$, where the source \mathbf{r}_{src} is located away from the given stencil [3], etc.

stencils can be strongly distorted and unreliable [8]; including more nodes in the stencil tends to increase robustness.

The disparity between the desirable number of basis functions and stencil nodes became particularly apparent in three-dimensional electromagnetic vector problems. If the number of basis functions is commensurate with the number of the nodal degrees of freedom (number of stencil nodes times three Cartesian components), the basis sets become ill-conditioned. Pinheiro & Webb recently overcame this difficulty by using a relatively small number of approximating functions and applying a least-squares match of the nodal values [9]. It is this idea that is further advanced in the present paper.

The use of least squares matching allows one to relax or even sever the connection between the basis functions and the stencil. This facilitates the construction of FLAME on non-canonical irregular stencils. So far FLAME has mostly been used on regular Cartesian grids – not as a requirement but as a practical matter, to avoid dealing with distorted / skewed stencils. An exception to this practice was adaptive FLAME in [8], where complications due to irregular distributions of nodes in adaptive refinement stencils had to be overcome.

Irregular and adaptive node arrangements are in general highly desirable because the nodes can be concentrated in areas where they are needed the most, in contrast with a regular grid that can only be refined globally. The least squares FLAME described in this paper works on non-canonical stencils more reliably than the previous versions of FLAME.

Irregular stencils are clearly a feature that the new approach, least-squares FLAME, shares with meshless methods (see reviews [10,11]). Another feature that is shared – albeit superficially (see below) – is the least squares matching. I shall, however, refrain from referring to least squares FLAME as a meshless method, for the following reasons.

The primary and defining feature of FLAME is the accurate Trefftz approximation; “meshlessness” is secondary. Approaches that have come to be known as “meshless methods” are associated with quite different approximations. Moving least squares (MLS) techniques, the “reproducing kernel particle method” (RKPM) [11,13,10], and, most recently, maximum-entropy approximations [16,17] are part and parcel of meshless techniques but are quite foreign to FLAME.

Also, the similarity between least squares FLAME and the established meshless methods does not go very far. MLS, RKPM or maximum-entropy functions in meshless methods are subject to costly numerical integration and differentiation. In contrast, no integration or differentiation is needed in FLAME at all.

The use of the least squares fit in both MLS and FLAME is also a superficial similarity. In MLS, the approximation is “moving,” in the sense that the coefficients of the relevant polynomial expansion vary from point to point and are found via a least squares match at the nodes. The spatial variation of the coefficients complicates the differentiation and integration that need to be carried out in the numerical procedure. In FLAME, the

approximation is usually non-polynomial and “static”: the coefficients are fixed for any given stencil. Further notes on meshless methods can be found in Section 6.

Connections of FLAME with other classes of numerical methods such as variational Trefftz methods, GFEM, Discontinuous Galerkin, variational-difference schemes by Moskow *et al.* [18], discontinuous enrichment and others have previously been discussed in great detail [1]; see in particular Sections 1 & 2, Fig. 1, and references in that paper. Here I briefly comment on a few additional contributions, some of them recent.

There is a well established and respectable body of work on special high-order schemes for various types of problems, in particular the Helmholtz equation [19, 20, 21, 22, 23, 24]; see Harari’s review [19] for further information and references. There is a commonality of goals but not of the methodology between these techniques and FLAME.

Special difference schemes that can now be viewed as natural particular cases of FLAME have been independently invented by various research groups. Mei [25] used the fundamental solutions of the Laplace equation to construct approximate absorbing conditions at the exterior boundary of the computational domain for unbounded problems. Similar ideas were put forward by Mittra, Boag and Leviatan [26, 28, 27]. Hadley [29, 30] derives difference schemes for the Helmholtz equation (with applications to electromagnetic waveguide analysis) from the Bessel function expansion in free space as well as at material boundaries and corners. Very recently, Chiang and co-authors [31, 32] developed high-order schemes for frequency domain analysis of 2-D photonic crystals; to do so, they carefully match first and higher order derivatives at curved dielectric interfaces. Also in connection with photonic crystals, Lu *et al.* proposed a pseudospectral method of Dirichlet-to-Neumann (DtN) maps [33, 34], where the field is approximated by cylindrical harmonics within the lattice cell and the Bloch-Floquet conditions are imposed at a set of boundary collocation points. FLAME, unlike DtN, relies only on *local* analytical approximations over a given stencil, which tends to be computationally more stable than approximations over the whole lattice cell [7].

The remainder of the paper is organized as follows. For completeness, Section 2 summarizes the established FLAME setup. Section 3 presents the new version of FLAME that casts the idea of Pinheiro & Webb in a general form. As explained in Section 4, boundary conditions in FLAME are easy to impose. Section 5 proves that the consistency error in FLAME is commensurate with the approximation accuracy of the solution by the FLAME bases.

A brief review of meshless methods, in comparison with the least squares FLAME, is given in Section 6. A variety of numerical examples in 2D and 3D (Section 7) include electrostatic (magnetostatic) particle interactions, scattering of electromagnetic (or acoustic) waves, and wave propagation in a photonic crystal. The examples also explore the role of the grid and stencil

size, of the number of approximating functions, and of the irregularity of the stencils.

2 Trefftz-FLAME Schemes: A Brief Review

Trefftz-FLAME is a generalized finite-difference (FD) calculus that incorporates accurate local approximations of the solution into a difference scheme. Conceptually, the computational domain Ω is covered by a finite number of overlapping subdomains (“patches”) $\Omega^{(i)}$, $\Omega = \cup \Omega^{(i)}$, $i = 1, 2, \dots, n$. Each patch contains a stencil of a global Cartesian grid.

Associated with each patch $\Omega^{(i)}$ is the local approximation space

$$\Psi^{(i)} = \text{span}\{\psi_\alpha^{(i)}\}, \quad \alpha = 1, 2, \dots, m \quad (1)$$

The number m of approximating functions and the number M of stencil nodes may in general depend on the patch, but for simplicity of notation this is not explicitly indicated; i.e. we write M, m instead of $M^{(i)}, m^{(i)}$. Superscript (i) will occasionally be dropped in other cases as well, when it is clear from the context that the focus is on a particular patch (stencil) and there is no possibility of confusion.

The local solution $u_h^{(i)}$ lies in space $\Psi^{(i)}$ – i.e. it is a linear combination of the local basis functions

$$u_h^{(i)} = \sum_{\alpha=1}^m c_\alpha^{(i)} \psi_\alpha^{(i)} \quad (2)$$

In Trefftz-FLAME, the basis functions are chosen to satisfy the underlying differential equation, along with the interface boundary conditions.

Clearly, the the nodal values $\underline{u}^{(i)} \in \mathbb{R}^M$ of function $u_h^{(i)}$ on stencil $\#i$ are linearly related to the coefficient vector $\underline{c}^{(i)} \equiv \{c_\alpha^{(i)}\} \in \mathbb{R}^m$. The relevant transformation matrix $N^{(i)}$,

$$\underline{u}^{(i)} = N^{(i)} \underline{c}^{(i)} \quad (3)$$

contains the nodal values of the basis functions on the stencil; if r_k is the position vector of node k , then [1, 2, 4]

$$N^{(i)} = \begin{pmatrix} \psi_1^{(i)}(r_1) & \psi_2^{(i)}(r_1) & \dots & \psi_m^{(i)}(r_1) \\ \psi_1^{(i)}(r_2) & \psi_2^{(i)}(r_2) & \dots & \psi_m^{(i)}(r_2) \\ \dots & \dots & \dots & \dots \\ \psi_1^{(i)}(r_M) & \psi_2^{(i)}(r_M) & \dots & \psi_m^{(i)}(r_M) \end{pmatrix} \quad (4)$$

A coefficient vector $\underline{s}^{(i)} \in \mathbb{R}^M$ is sought to yield the difference scheme

$$\underline{s}^{(i)T} \underline{u}^{(i)} = 0 \quad (5)$$

for the nodal values $\underline{u}^{(i)}$ of *any* function $u_h^{(i)}$ of form (2). Due to (3) and (5),

$$\underline{s}^{(i)T} N^{(i)} \underline{c}^{(i)} = 0 \quad (6)$$

For this to hold for any set of coefficients $\underline{c}^{(i)}$, one must have

$$\underline{s}^{(i)} \in \text{Null}(N^{(i)T}) \quad (7)$$

We shall assume that the stencil and the basis set are such that the null space in the definition of the scheme is of dimension one. If this happens not to be the case in a particular situation, the stencil and/or the basis set need to be changed.

For *inhomogeneous* equations (i.e. with a nonzero right hand side) of the generic form

$$\mathcal{L}u = f, \quad (8)$$

FLAME schemes are generated by introducing the local splitting of the solution:

$$u^{(i)} = u_0^{(i)} + u_f^{(i)}, \quad (9)$$

where $u_0^{(i)}$ is the solution for the homogeneous equation and $u_f^{(i)}$ is a particular solution of the inhomogeneous equation. The inhomogeneous FLAME scheme is [1, 4]

$$\underline{s}^{(i)T} \underline{u}^{(i)} = \underline{s}^{(i)T} \underline{u}_f^{(i)} \quad (10)$$

The coefficients of the scheme and hence the system matrix are the same for the homogeneous and inhomogeneous problems. The difference is that, in the presence of sources in the vicinity of a given grid stencil, the right hand side is formed, as indicated by (10), by applying the difference operator to the nodal values of the particular solution $u_f^{(i)}$.

3 New Schemes: Least Squares Trefftz-FLAME

This section formalizes the modification of FLAME proposed by Pinheiro & Webb [9] and casts it in a general form. Specific examples are presented in the following sections.

One again formally considers a cover $\cup \Omega^{(i)}$, $i = 1, 2, \dots, n$ of the computational domain by overlapping patches $\Omega^{(i)}$. Each patch again contains a set of nodes (stencil). We do not have to assume a regular underlying grid; the nodes could form fuzzy “clouds”.

The local approximation spaces are introduced in exactly the same way as previously; to repeat for easy reference,

$$\Psi^{(i)} = \text{span}\{\psi_\alpha^{(i)}\}, \quad \alpha = 1, 2, \dots, m \quad (11)$$

As before, the local solution $u_h^{(i)}$ lies in $\Psi^{(i)}$ – i.e. it is a linear combination of the local basis functions satisfying the underlying differential equation, along with the interface boundary conditions:

$$u_h^{(i)} = \sum_{\alpha=1}^m c_\alpha^{(i)} \psi_\alpha^{(i)} \quad (12)$$

At this point, the new approach parts ways with the established version of FLAME and involves, formally, *two* sets of points. The first one is $n^{(i)}$ stencil nodes $\mathcal{S}^{(i)}$ for which the difference scheme is being generated, and the other one is a reduced set $\mathcal{S}_1^{(i)} \subset \mathcal{S}^{(i)}$ of $n_1^{(i)} < n^{(i)}$ nodes at which least squares matching of the solution is effected, as described below. In practice, the two sets will typically differ just by one extra node in $\mathcal{S}^{(i)}$ (see below).

For any given set of nodal values on the reduced set $\mathcal{S}_1^{(i)}$, the linear relationship (3) between these values and the expansion coefficients is required to be satisfied in the least squares (l.s.) sense rather than exactly:

$$\underline{u}_{\mathcal{S}_1}^{(i)} \stackrel{l.s.}{=} N_1^{(i)} \underline{c}^{(i)} \quad (13)$$

Here $N_1^{(i)}$ is the matrix of nodal values of the basis functions on $\mathcal{S}_1^{(i)}$ – a matrix completely analogous to $N^{(i)}$ of the previous section. The advantage of using the least squares match is that, as already noted, the connection between the set of basis functions and the stencil becomes much less rigid than in the established version of FLAME.

More explicitly, the least squares relationship can be written as

$$\underline{c}^{(i)} = N_1^{(i)+} \underline{u}_{\mathcal{S}_1}^{(i)} \quad (14)$$

where $N_1^{(i)+}$ is the generalized inverse (also known as the pseudoinverse or the Moore-Penrose inverse)

$$N_1^{(i)+} = \left(N_1^{(i)T} N_1^{(i)} \right)^{-1} N_1^{(i)T} \quad (15)$$

assuming that the matrix in the parentheses is nonsingular. This expression comes directly from the least squares methodology.²

The nodal values on the remaining subset of the stencil nodes $\mathcal{S}_0^{(i)} = \mathcal{S}^{(i)} - \mathcal{S}_1^{(i)}$ are required to be *exactly* representable – as opposed to the least-squares fit – by a linear combination of the basis functions. Then the Euclidean vector of these nodal values is

$$\underline{u}_{\mathcal{S}_0}^{(i)} = N_0^{(i)} \underline{c}^{(i)} = N_0^{(i)} N_1^{(i)+} \underline{u}_{\mathcal{S}_1}^{(i)} \quad (16)$$

where $N_0^{(i)}$, directly analogous to $N_1^{(i)}$, contains the values of the basis functions on the nodes of $\mathcal{S}_0^{(i)}$. For a homogeneous differential equation

² It is well known that matrix inversion is hardly ever needed in practical computation. In particular, the pseudoinverse can be computed using the QR method rather than by explicit matrix inversion.

(zero right hand side), we are again looking for a coefficient vector $\underline{s}^{(i)}$ of the difference scheme

$$\underline{s}^{(i)T} \underline{u}^{(i)} = 0 \quad (17)$$

or, equivalently due to (16)

$$\underline{s}^{(i)T} \begin{pmatrix} N_0^{(i)} N_1^{(i)+} \\ I_{n_1} \end{pmatrix} \underline{u}_{S_1}^{(i)} = 0 \quad (18)$$

where I_{n_1} is the $n_1 \times n_1$ identity matrix. A natural partitioning of the difference scheme $\underline{s}^{(i)T} = (\underline{s}_0^{(i)T}, \underline{s}_1^{(i)T})$ is assumed, with the coefficients $\underline{s}_0^{(i)T}, \underline{s}_1^{(i)T}$ corresponding to the nodes in $S_0^{(i)}$ and $S_1^{(i)}$, respectively.

Since the vector of nodal values $\underline{u}_{S_1}^{(i)}$ is unknown and in a sense quasi-arbitrary, we require that the above relationship be satisfied for any such vector. This immediately gives

$$\underline{s}^{(i)} \in \text{Null} \begin{pmatrix} N_0^{(i)} N_1^{(i)+} \\ I_{n_1} \end{pmatrix}^T \equiv \text{Null} \begin{pmatrix} N_1^{(i)+T} N_0^{(i)T}, & I_{n_1} \end{pmatrix} \quad (19)$$

This is our main expression generalizing the null space condition (7) of the established version of Trefftz-FLAME. We shall always assume that the stencil and the basis are set up in such a way that the null space in the definition of the scheme is of dimension one. Otherwise the basis and/or the stencil need to be modified.

It immediately follows from (19) that the scheme can be explicitly written as

$$\underline{s}^T = (s_0^{(i)T}, -s_0^{(i)T} N_0^{(i)} N_1^{(i)+}) \quad (20)$$

Typically $S_0^{(i)}$ will contain only one node, in which case, since the null space is defined up to an arbitrary factor, one can set $s_0^{(i)} = 1$ and obtain

$$\underline{s}^{(i)T} = (1, -N_0^{(i)} N_1^{(i)+}) \quad (21)$$

This is equivalent to Pinheiro & Webb's algorithm that they used for electromagnetic wave scattering in 3D [9].

The rectangular matrix on the right of (19) has the number of columns equal to the stencil size $n^{(i)}$ and the number of rows equal to the number of nodes $n_1^{(i)}$ in the substencil $S_1^{(i)}$. Ordinarily, such a matrix will have a one-dimensional nullspace (leading to a unique FLAME scheme) if the numbers of columns and rows differ by one – that is, if $n_1^{(i)} = n^{(i)} - 1$ and $S_0^{(i)}$ has exactly one node, as stipulated above.

For convenience, Figs. 1–4 illustrate the dimensions and composition of the matrices involved in the key equations from (14) to (19). In this illustration, there are four approximating functions and seven stencil nodes, five of which are the “least squares” matching nodes of S_1 . Although one node rather than two would be typical for S_0 , two nodes are assumed, to demonstrate the general principle.

$$\underline{c}^{(i)} = N_1^{(i)+} \underline{u}_{S1}^{(i)}$$

Fig. 1 Matrix dimensions in (14) for $n_1^{(i)} = 5$, $m = 4$.

$$\underline{u}_{S0}^{(i)} = N_0^{(i)} \underline{c}^{(i)} = N_0^{(i)} N_1^{(i)+} \underline{u}_{S1}^{(i)}$$

Fig. 2 Matrix dimensions in (16) for $n_1^{(i)} = 5$, $n^{(i)} = 7$, $m = 4$.

$$\underline{s}^{(i)T} \begin{bmatrix} N_0^{(i)} & N_1^{(i)+} \\ \vdots & \vdots \\ I_{n1} \end{bmatrix} \underline{u}_{S1}^{(i)} = 0$$

Fig. 3 Matrix dimensions and structure in (18) for $n_1^{(i)} = 5$, $n^{(i)} = 7$.

4 Boundary Conditions in FLAME

Boundary conditions at the material boundaries are built into the Trefftz-FLAME bases and therefore need no other treatment, in sharp contrast with the methods where smooth functions not obeying the boundary conditions are employed (e.g. MLS or radial basis functions). Exterior boundary conditions in FLAME do not pose any problem either. Since all approximations are local, approximations near exterior boundaries are completely decoupled from approximations elsewhere. In fact, any traditional non-FLAME

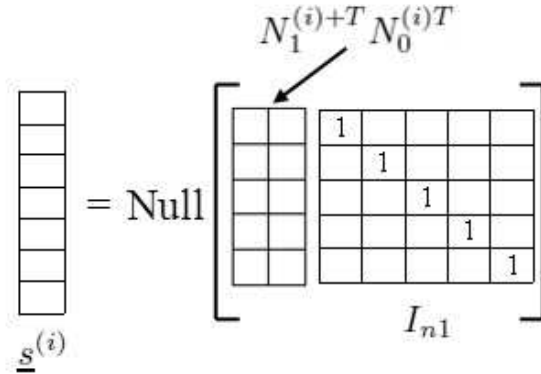


Fig. 4 Matrix dimensions and structure in (19) for $n_1^{(i)} = 5$, $n^{(i)} = 7$.

schemes, including perfectly matched layers (PML), can be used at the boundaries. One could also opt for FLAME schemes at the boundary – the FLAME PML [2, 4] being one example.

Natural boundary conditions (Neumann and the like) can either be handled in the established ways by traditional schemes or, alternatively, using FLAME with a subset of Trefftz functions satisfying the natural conditions.

In the customary algorithmic implementation of Dirichlet conditions, one initially disregards the distinction between the nodes at the exterior boundary and the inner nodes. Then, after the system matrix has been assembled, the usual adjustments are made: terms of the form $a_{ij}u_j$, where u_j is a given Dirichlet value and a_{ij} is a matrix entry, are moved over to the right hand side. The entry in the right hand side is modified accordingly and the matrix entry a_{ij} is then set to zero.

Even “fuzzy” exterior boundaries, where the diffuse set of nodes does not fall exactly on a predefined surface, could be handled in the same fashion. There may be some redundancy if the fuzzy boundary layer is slightly “thicker” than necessary in some places. It is trivial but optional to eliminate the redundant nodes (for example, the ones connected only to other Dirichlet nodes) from the system.

5 Consistency Error of FLAME

Analysis of the consistency error of least squares FLAME proceeds along the same lines as in the original version of FLAME [1, 2], with some modifications. Here we shall only consider equations with the zero right hand side in a given patch (i.e. over a given grid stencil); the treatment of equations with nonzero r.h.s. is exactly the same as in the established versions of FLAME [1, 2].

The consistency error of scheme (17), (21) is, by definition, obtained by substituting the nodal values of the exact solution u^* into (17). Let $\epsilon_a(h)$

be the approximation error of the exact solution u^* within a patch $\Omega^{(i)}$:

$$\epsilon_a(h) = \min_{\underline{c}^{(i)} \in \mathbb{R}^m} \left\| u^* - \sum_{\alpha=1}^m c_\alpha^{(i)} \psi_\alpha^{(i)} \right\|_\infty \quad (22)$$

Equivalently, there exists a coefficient vector $\underline{c}^{(i)} \in \mathbb{R}^m$ such that

$$u^* = \sum_{\alpha=1}^m c_\alpha^{(i)} \psi_\alpha^{(i)} + \eta, \quad \|\eta\|_\infty = \epsilon_a(h) \quad (23)$$

within the patch. For the nodal values, one then has due to (16)

$$\mathcal{N}^{(i)} u^* = N^{(i)} \underline{c}^{(i)} + \underline{\eta} \quad (24)$$

where $\mathcal{N}^{(i)} u^*$ and $\underline{\eta} = \mathcal{N}^{(i)} \eta$ are the Euclidean vectors of nodal values of the exact solution and of η over stencil i , respectively. $N^{(i)}$ is (as always) the matrix of nodal values of the basis functions. Due to (23),

$$\|\underline{\eta}\|_\infty \leq \epsilon_a(h)$$

In particular, for the nodal values on the “least squares part” $S_1^{(i)}$ of the stencil, we have

$$\underline{u}_1^{*(i)} = N_1^{(i)} \underline{c}^{(i)} + \underline{\eta}_1 \quad (25)$$

Left-multiplying this equation with $N_1^{(i)T}$ and then expressing $\underline{c}^{(i)}$ yields

$$\underline{c}^{(i)} = \left(N_1^{(i)T} N_1^{(i)} \right)^{-1} N_1^{(i)T} (\underline{u}_1^{*(i)} - \underline{\eta}_1) \equiv N_1^{(i)+} (\underline{u}_1^{*(i)} - \underline{\eta}_1) \quad (26)$$

assuming that the matrix in the parentheses is nonsingular. The i th component of the consistency error for scheme (21) is, by definition,³

$$\begin{aligned} |\epsilon_{ci}(h)| &= \left| \underline{c}^{(i)T} \mathcal{N}^{(i)} u^* \right| = \left| u_0^* - N_0^{(i)} N_1^{(i)+} N_1^{(i)} u_1^* \right| \\ &= \left| (N_0^{(i)} \underline{c}^{(i)} + \eta_0) - N_0^{(i)} N_1^{(i)+} (N_1^{(i)} \underline{c}^{(i)} + \underline{\eta}_1) \right| \end{aligned}$$

Now substituting $\underline{c}^{(i)}$ from (26), we have

$$\begin{aligned} |\epsilon_{ci}(h)| &= \left| \left[N_0^{(i)} N_1^{(i)+} - N_0^{(i)} N_1^{(i)+} N_1^{(i)} N_1^{(i)+} \right] (\underline{u}_1^{*(i)} - \underline{\eta}_1) + \eta_0 \right. \\ &\quad \left. - N_0^{(i)} N_1^{(i)+} \underline{\eta}_1 \right| = \left| \eta_0 - N_0^{(i)} N_1^{(i)+} \underline{\eta}_1 \right| \leq |\eta_0| + \left\| N_0^{(i)} N_1^{(i)+} \right\| \|\underline{\eta}_1\| \quad (27) \end{aligned}$$

where the term in the square brackets has in the end vanished because $A^+ A A^+ = A^+$ for any pseudoinverse matrix A^+ . As a result of the generalized inverse falling out of the accuracy estimate, it can be seen – somewhat counterintuitively – that the least squares fit does *not* reduce the accuracy as compared to the exact nodal match. The consistency error is still governed primarily by the approximation error.

³ Analysis for the slightly more general scheme (20) is similar.

6 Trefftz-FLAME vs. Meshless Methods

Meshless methods have been developed and studied very extensively over the last two decades, and excellent contributions and reviews [11, 12, 13, 14, 15], including a detailed recent one [10], are available. This section is limited to a brief summary of such methods, with the emphasis on some similarities with FLAME but – more importantly – on the differences.

Meshless techniques have two key advantages. One is, by definition, the absence of complex meshes that may be difficult to generate, especially in 3D, – although regular auxiliary grids are still needed to compute the numerical quadratures in weighted residual and Galerkin methods.

The second advantage is high-order approximation, at least in the regions where the solution is smooth. This can be accomplished by the Reproducing kernel particle method (RKPM), Moving least squares (MLS) or similar approximations, as well as by the recently developed maximum-entropy functions [16, 17].

However, meshless methods have problems that are, in a certain sense, an extension of their advantages. Approximation by smooth functions is accurate in homogeneous regions but breaks down at interface boundaries where the solution or its derivatives have jumps. The MLS, RKPM and similar approximating functions and especially their derivatives are too complex to be differentiated or integrated analytically. Therefore one has to resort to numerical integration and differentiation, which is in general quite costly. Not only interface boundary conditions but also the Dirichlet conditions on the exterior boundary of the domain are difficult to impose numerically because the basis function do not satisfy the Kronecker delta property at the nodes. The maximum-entropy functions of [16, 17] satisfy a “weak Kronecker delta” property due to their rapid decay; however, to compute these functions, one has to solve a nonlinear optimization problem.

These impediments and ways of getting around them have been the subject of much research that is still ongoing [10]. The difficulties can be alleviated but not removed. For example, if collocation instead of weighted residual / Galerkin methods is used, numerical integration becomes unnecessary but, as an unpleasant trade-off, higher-order derivatives, commensurate with the order of the differential operator, of the basis functions have to be calculated. (In the weighted residual methods, half of the derivatives are usually moved over from the basis functions to the test functions, thereby reducing the required order of differentiation. For collocation, this avenue is not available.)

Interface boundary conditions in meshless methods can be treated using Lagrange multipliers or by introducing additional “enrichment” functions. (The latter can also be used to represent boundary layers, singularities, etc.) This, however, increases the computational and algorithmic complexity. Lagrange multipliers not only constitute additional unknowns in the system but may also adversely affect the algebraic properties of the system and may lead to ill-conditioning. The enrichment functions may have to be mollified

by partition of unity factors (to make their support small) and then are also subject to numerical integration and differentiation.

In contrast, Trefftz-FLAME basis functions satisfy the underlying equation and the boundary conditions by construction and therefore do not require any additional constraints to be imposed. In essence, *all* FLAME functions are “enrichment” functions in the sense outlined above; all of them are physical and reflect the local behavior of the solution. No degrees of freedom are wasted on approximating broader classes of functions not directly relevant to the problem under consideration.

In short, the difficulties that traditional meshless methods have in dealing with interface and essential conditions are real, but ways have been developed to overcome that. FLAME does not have these difficulties to begin with, so there is nothing to overcome. The price to pay for this advantage is the need to pre-define accurate local analytical or semi-analytical bases. The complexity of this task depends on the class of problems, making FLAME quite suitable for some classes and less so for the others. Examples of problems where the new version of FLAME works well are presented in Section 7; see also [1, 2, 4, 5] for many other examples of the established version of FLAME.

7 Computational Examples of Trefftz-FLAME on Irregular Grids

7.1 2D Electromagnetic Wave Scattering

Let us start by applying least squares FLAME to the classical problem of electromagnetic scattering from a dielectric cylinder. Non-ideal conductors can be treated in the same manner as dielectrics if complex permittivity is used. The wave is assumed monochromatic

In the 2D case, where the material parameters and fields are independent of one coordinate (say, z), electromagnetic waves can be decomposed into two modes. In the E -mode (known as the s -mode in optics and frequently, but not always, also referred to as the TM mode) the electric field has only one component $E = E_z$, whereas the magnetic field \mathbf{H} has x and y components, with $H_z = 0$. Similarly, for the H -mode (also known as the p - or TE mode) $H = H_z$, $E_z = 0$. These modes satisfy the following equations that are easy to derive from Maxwell’s system:

$$\nabla \cdot \mu^{-1} \nabla E + \omega^2 \epsilon E = 0 \quad (28)$$

$$\nabla \cdot \epsilon^{-1} \nabla H + \omega^2 \mu H = 0 \quad (29)$$

For numerical testing, let us consider a dielectric cylinder of radius r_{cyl} and dielectric permittivity ϵ_{cyl} . The host medium is assumed to have the relative dielectric constant of one, $\epsilon_{\text{out}} = 1$. The incident field is a plane wave with a wave vector \mathbf{k} ,

$$\mathbf{E}_{\text{inc}} = \mathbf{E}_0 \exp(i\mathbf{k} \cdot \mathbf{r})$$

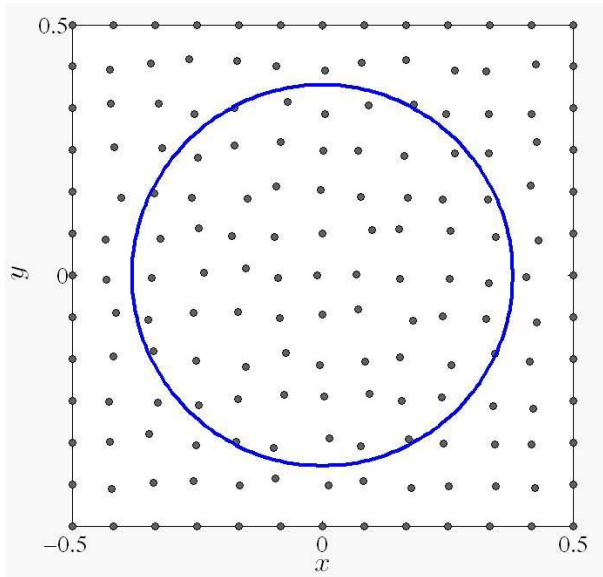


Fig. 5 An irregular 12×12 grid around a cylindrical scatterer. “Fuzziness” $f = 0.4$.

under the $\exp(-i\omega t)$ complex phasor convention. To complete the formulation, the standard Sommerfeld radiation conditions can be imposed on the scattered field $\mathbf{E}_{\text{sc}} = \mathbf{E} - \mathbf{E}_{\text{inc}}$. Numerically, well established techniques such as PML or absorbing boundary conditions can be applied on the exterior boundary. Since our focus is on the construction of accurate difference schemes in the interior, absorbing conditions are a tangential issue, and in the numerical tests the exact solution was imposed as a Dirichlet condition. (A textbook solution for a cylindrical scatterer can be found e.g. in [35].) When Dirichlet conditions are imposed, it is tacitly assumed that ω is not an eigenvalue of the corresponding operators $\nabla \cdot \mu^{-1} \nabla$ or $\nabla \cdot \epsilon^{-1} \nabla$.

The computational domain is normalized to the unit square $[-0.5, 0.5] \times [-0.5, 0.5]$. In all numerical experiments, the scatterer is centered at the origin and has the relative permittivity of $\epsilon_{\text{cyl}} = 9$ and radius $r_{\text{cyl}} = 0.25$.

Irregular grids are generated by randomly displacing the nodes of a regular Cartesian grid:

$$\hat{x}_i = x_i + f\eta_{xi}h_x \quad (30)$$

where x_i is the coordinate of the i th node of the regular grid, h_x is the grid size in the x -direction, η_{xi} is a random number uniformly distributed within $(-0.5, 0.5)$. Parameter f controls the “fuzziness” of the distribution and is chosen between 0 and 0.5, to maintain the majority of the topological connections between each node and its nearest neighbors. Displacements in the y direction are generated in a completely similar way. Fig. 5 gives an example of a 12×12 irregular grid.

Construction of the Trefftz bases has been elaborated upon in the previous publications [1, 2, 4, 5]. Briefly, the basis functions are chosen as cylindrical harmonics:

$$\begin{aligned}\psi_\alpha^{(i)} &= a_n J_n(k_{\text{cyl}} r) \exp(in\phi), \quad r \leq r_0 \\ \psi_\alpha^{(i)} &= [b_n J_n(k_{\text{air}} r) + H_n^{(1)}(k_{\text{air}} r)] \exp(in\phi), \quad r > r_0\end{aligned}$$

where J_n is the Bessel function, $H_n^{(1)}$ is the Hankel function of the first kind⁴, and a_n, b_n are coefficients found via the standard conditions on the boundary of the cylinder. The FLAME basis contains a finite number of harmonics from the monopole ($n = 0$) up to some highest order n_{max} .

The relative numerical errors for the E -mode computed on a 30×30 FLAME grid, with a varying number of basis functions, stencil nodes and fuzziness, are reported in Table 1. The stencil of size m for any given node is formally defined as the set of m nodes closest to that node (including the node itself). The relative errors were computed as

$$\delta_{\text{rel}} \equiv \frac{\|\underline{u}_{\text{FLAME}} - \underline{u}_{\text{exact}}\|}{\|\underline{u}_{\text{exact}}\|} \quad (31)$$

The overall high accuracy of FLAME is evident from the table. Five to ten correct digits in the value of the field are routinely obtained, even though the grid is irregular, relatively coarse and *does not represent the geometry* of the problem in any way. Rather, the geometric and physical information is built into the FLAME bases.

While the high accuracy was to be expected, there are two surprises in the results of Table 1. First, the fuzziness of the grid does not significantly affect the accuracy – if anything, the errors on fuzzier grids ($f = 0.2, f = 0.4$) tend to be a little lower than on the regular one ($f = 0$). No “physical” reason for that is apparent, especially in light of the fact that the situation in 3D is different (see the 3D example below).

The second surprise is that, while the accuracy improves as expected when the number of multipoles n_{max} is increased from three to four to five, the relative error goes up from $\sim 10^{-11}$ to $\sim 10^{-10}$ when the 6th order multipoles are included. One possible circumstance that might contribute to this was noted by Čajko [36]: the coefficients of high-order schemes must themselves be computed with very high precision, to avoid an asymptotic loss of accuracy for fine grids.

7.2 Wave Propagation in Photonic Crystals

Photonic crystals (PhC) are artificial periodic structures that exhibit very peculiar characteristics of wave propagation (e.g. the photonic bandgap [37,

⁴ Hankel functions of the *second* kind should be used if the $\exp(i\omega t)$ phasor convention common in electrical engineering is adopted.

n_{\max} (highest harmonic in the FLAME basis)	Stencil size	“Fuzziness factor” f	Numerical error
3	9	0	1.1E-06
4	13	0	2.3E-09
5	21	0	1.29E-11
6	21	0	4.5E-10
3	9	0.2	1.1E-06
4	13	0.2	6.2E-11
5	21	0.2	1.5E-11
6	21	0.2	3.6E-10
3	9	0.4	8.7E-07
4	13	0.4	7.3E-11
5	21	0.4	1.3E-11
6	21	0.4	4.7E-10

Table 1 Relative numerical errors in the nodal values of the electric field for least squares FLAME schemes with varying bases and stencils on a 30×30 grid. Scattering from a dielectric cylinder with $\epsilon_{\text{cyl}} = 9$, $r_{\text{cyl}} = 0.25$.

38,39,40]) and are finding various applications in lightwave technology [41, 42,2]. Our goal here is limited to using PhC as a demonstration example for the new version of FLAME.

For convenience of comparison, consider the same numerical example as in [2,4]: a photonic crystal due to Fujisawa & Koshiba [43], with a square lattice of cylindrical coaxial dielectric rods and a bended waveguide obtained by eliminating a few of these rods (Fig. 6). The E - and H -modes of the wave are governed by equations (28) and (29), respectively.

As in the previous tests [2,4], the dielectric constant is set to $\epsilon_{\text{rod}} = 9$ for the rods (index of refraction $n = 3$) and to unity for the outside medium. The radius of the cylinders and the wavenumber are normalized to unity; the air gap between the neighboring rods is equal to their radius. The field distribution is shown in Fig. 6 for illustration. Simplified boundary conditions are set equal to an externally applied plane wave. This is adequate for the demonstration example; conditions at the ports of the guide are a separate issue, and a way to handle them in FLAME was developed by Pinheiro & Webb [44].

An excellent agreement between the established version of Trefftz-FLAME and independent FEM simulations has been previously demonstrated [2,4]; in fact, numerical evidence was convincing that the numerical error was in this case orders of magnitude lower in FLAME than in FEM with a comparable number of unknowns.

Our goal here is to compare the least squares FLAME on fuzzy node clouds with the previous Trefftz-FLAME on regular Cartesian grids, thereby exploring the influence of the “fuzziness” on the numerical accuracy. The “fuzzy” node coordinates \hat{x}_i , \hat{y}_i are generated as in (30). Fig. 7 shows an

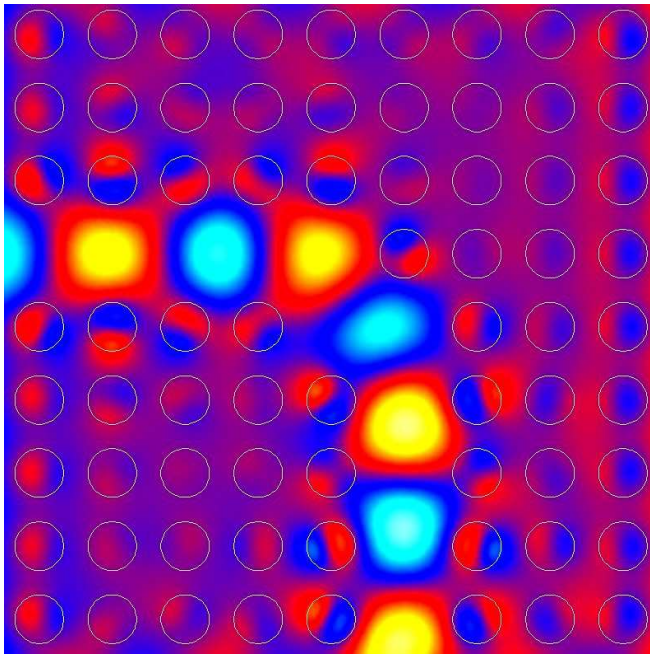


Fig. 6 The imaginary part of the electric field in the photonic crystal waveguide bend. The real part looks qualitatively similar. (Reprinted by permission from [4] ©2005 IEEE.)

example of an irregular 60×60 FLAME grid with the “fuzziness factor” $f = 0.4$.

This grid was used to produce the least squares FLAME results in Fig. 8, where the distribution of the electric field along the midline of the crystal ($y = 0$) is shown for the E -mode. The result obtained with the new version of FLAME coincides with the various results obtained previously with FEM and FLAME, despite the quite irregular distribution of nodes in the new test (see Fig. 7).

Note that for the 60×60 grid there are about 12.5 points per wavelength (ppw) in the air but only 4.2 ppw in the rods, and yet the FLAME results are very accurate even on an irregular grid, due to the Trefftz approximation. Alternative methods that rely on generic polynomial approximations would require a substantially higher number of ppw to achieve the same accuracy.

The FLAME field values plotted in Fig. 8 were produced by interpolation, similar to the way described in [2], pp. 290–291, for the previous version of FLAME. Namely, for a given set of nodal values on a stencil, one finds the Trefftz expansion coefficients $c^{(i)}$ by solving the least squares problem either on the substencil S_1 (13) or, alternatively, on the whole stencil. The interpolation is then effected by the Trefftz expansion (2).

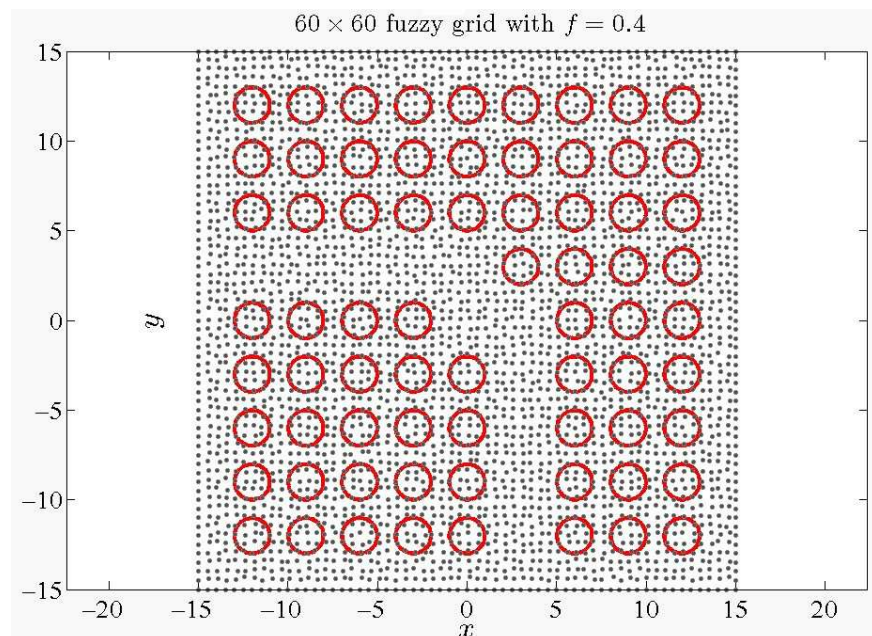


Fig. 7 A 60×60 irregular FLAME grid in the photonic crystal example. “Fuzziness factor” $f = 0.4$.

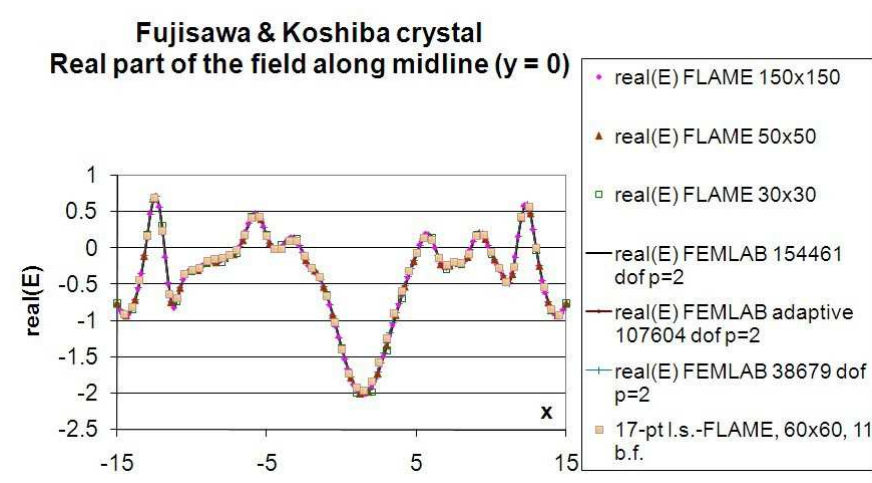


Fig. 8 Field distribution in the Fujisawa–Koshiba photonic crystal along the central line $y = 0$. Solution by the new version of FLAME coincides with the previous FEM and FLAME results, despite the quite irregular distribution of nodes in the new test. For testing, least-squares FLAME was applied on 17-point stencils with 11 basis functions.

7.3 Electrostatic Particle Interactions in 3D

7.3.1 Formulation and setup. The 3D numerical example, chosen to be simple enough for illustration but extendable to more complex cases, involves two spherical dielectric particles in a uniform external electrostatic field.

A uniform field induces only the dipole mode in a *single* particle [35], but for two or more particles higher-order multipoles do arise. A semi-analytical solution can be obtained by the well known multipole-multicenter method (mmc) [45, 46, 2], where the potential is sought as a superposition of multipole expansions centered on each of the particles. To impose the boundary conditions on any given particle, one needs to translate the multipole expansions from all other particles to that particle; this is accomplished by the standard multipole translation formulas (e.g. [45]). Since the details of this procedure are easily found in the literature and are tangential to the subject matter of this paper, they are omitted here.

The electrostatic equation in terms of the total electric potential u is⁵

$$\nabla \cdot \epsilon \nabla u = 0; \quad u(\mathbf{r}) - u_{\text{ext}}(\mathbf{r}) \rightarrow 0 \quad \text{as } r \rightarrow \infty \quad (32)$$

where $u_{\text{ext}}(\mathbf{r})$ is the applied (external) potential, which for a uniform field is a linear function of coordinates. If understood in the sense of distributions, (32) implicitly includes the standard conditions on interface boundaries: the continuity of the potential and the normal component of the electric flux density $\mathbf{D} = \epsilon \mathbf{E}$. The div-grad equation (32) can also be rewritten in terms of the “scattered” potential $u_s \equiv u - u_{\text{ext}}$, but there is no particular need to do so here.

The construction of FLAME bases is analogous to the cylindrical case and involves spherical harmonics defined inside and outside a given particle and matched at its interface. Details can be found in [4, 2]. It is possible to increase the accuracy of FLAME by using more complex mmc bases over several neighboring particles as done in [8]; however, in this paper single-center basis functions are used for the sake of practical simplicity.

The mmc expansion with a large number of harmonics (64 terms per particle in the expansion) is used to compute a quasi-analytical solution for reference and error analysis.

The two spherical particles in our 3D example have radii $r_1 = 1$ and $r_2 = 1.25$ and are centered on the z axis at points $z_1 = -2.5$, $z_2 = 2$, respectively. The lack of geometric symmetry is deliberate, to avoid any computationally favorable artifacts due to symmetry. The dielectric constants inside and outside the particles in all numerical experiments were chosen as $\epsilon_{\text{in}} = 5$, $\epsilon_{\text{out}} = 1$, respectively. A cubic computational domain of size $L_{\text{dom}} = 10$ centered at the origin was used.

⁵ u is used instead of the somewhat more conventional ϕ to avoid confusion with the polar coordinate.

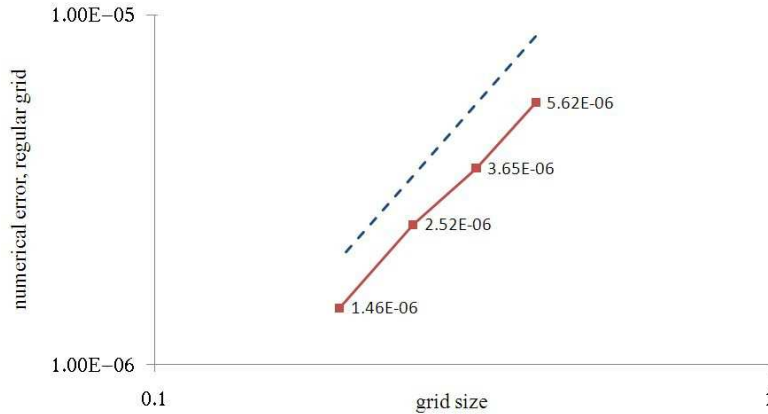


Fig. 9 Relative error in potential, regular grids. 19-point least-squares FLAME with 9 basis functions. Test for two spherical particles. To evaluate the numerical error, the mmc solution with 64 terms per particle was taken as quasi-exact. The dashed line is a visual aid indicating the $\mathcal{O}(h^2)$ convergence rate.

7.3.2 Regular Cartesian grids. The first set of tests is performed on regular Cartesian grids. The relative simplicity of this example notwithstanding, note that the regular grids do *not* carry any accurate geometric information about the shapes of the particles; that information is implicitly imbedded in the FLAME approximating functions. In contrast with the established version of FLAME, now the stencil size is to a large degree independent of the number of basis functions.

Fig. 9 illustrates convergence of 19-point least squares FLAME with nine basis functions. The relative error plotted in the figure was calculated as

$$\delta_{\text{rel}} \equiv \frac{\|\underline{u}_{\text{FLAME}} - \underline{u}_{\text{mmc}}\|}{\|\underline{u}_{\text{mmc}}\|} \quad (33)$$

where $\underline{u}_{\text{FLAME}}$ and $\underline{u}_{\text{mmc}}$ are Euclidean vectors of the nodal values of FLAME and mmc potentials, respectively; the norms are Euclidean.

The dashed line in Fig. 9 is a visual aid indicating the $\mathcal{O}(h^2)$ slope and demonstrating quadratic convergence, consistent with the number of basis functions (nine) used.

7.3.3 Irregular stencils. A fragment of an irregular distribution of nodes near one of the two particles is shown in Fig. 10. The random displacements of the nodes are generated in the same manner as in the previous examples, except that now these displacements are also applied in the z direction in addition to x and y . The exact potential was imposed as the Dirichlet boundary condition for testing, to avoid any extraneous errors due to domain truncation.

Table 2 demonstrates the effect of “fuzziness” on the numerical accuracy. For all combinations of basis functions and stencils in the table, the

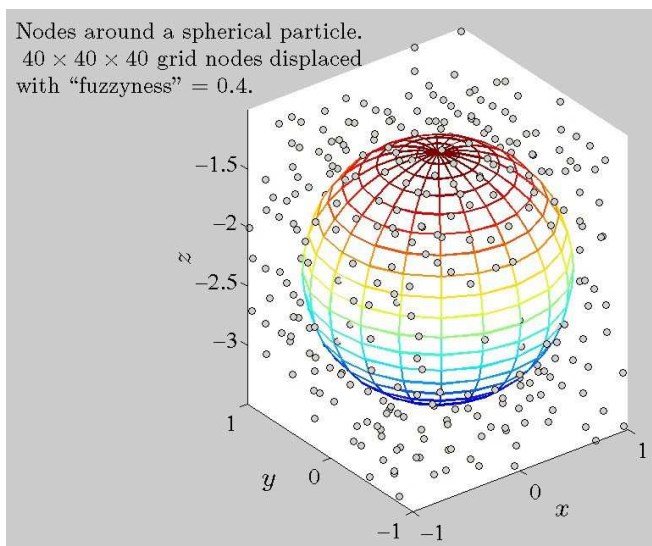


Fig. 10 An irregular set of nodes for FLAME in the vicinity of a particle. The nodes are randomly displaced with respect to the regular Cartesian grid $40 \times 40 \times 40$, with the “fuzziness” (see text) of $f = 0.4$. Nodes inside the particle not visible but are distributed in a similar manner and with the same density.

Number of basis functions	Stencil size	$f = 0$	$f = 0.1$	$f = 0.2$	$f = 0.4$
6	9	7.9E-04	8.05E-05	1.22E-04	2.69E-04
6	19	4.72E-06	5.31E-06	1.06E-05	2.49E-05
6	27	9.69E-06	9.17E-06	1.67E-05	1.74E-05
9	19	2.13E-06	2.00E-06	3.10E-06	9.17E-06
9	27	1.14E-05	1.12E-05	9.84E-06	6.68E-06

Table 2 Relative errors in the nodal potential for FLAME on irregular grids. The reference quasi-analytical solution obtained by the multipole-multicenter (mmc) expansion with 64 terms per particle. The 3D test problem with two dielectric particles with the dielectric permittivity 5. 41^3 nodes in FLAME.

numerical accuracy deteriorates somewhat as the “fuzziness” f increases. This is different from the previous 2D example where the fuzziness was not a significant factor.

The influence of the *stencil size* for a fixed number of basis functions is less straightforward. For six basis functions, the accuracy tends to improve when the stencil size changes from 9 to 19 but deteriorates somewhat as the stencil expands further.

A plausible qualitative explanation is as follows. As the number of stencil nodes increases, so does the robustness of the analytical approximation in FLAME, because more information (in the form of the nodal values) is being utilized. On the other hand, as the geometric size $\text{diam}(\Omega^{(i)})$ of the stencil

“patch” increases, the approximation accuracy, proportional to $\text{diam}(\Omega^{(i)})^p$, deteriorates (p is the order of approximation). These two conflicting trends lead to the nontrivial dependence of the accuracy on the stencil size. It would be worthwhile to analyze this rigorously in the future.

7.3.4 Random nodes. Further pushing the envelope, I have tested a completely random distribution of nodes (as opposed to random displacements around a regular lattice), see Fig. 11. Clearly, this can be viewed as the worst case scenario, and much better results can be expected if sensible adaptive procedures [8] are adopted in the future.

The initial test is performed with one particle only. In this case, since the exact solution contains only the dipole harmonic and is thus included in the FLAME basis, one can expect that FLAME will produce the exact solution up to the round-off error. This has been confirmed experimentally. For example, for 5000 FLAME nodes and the 27-point FLAME scheme with 16 basis functions, the relative error in the potential at the nodes was on the order of 10^{-13} , despite the fact that the distribution of the nodes is random and hence carries no geometric information whatsoever.

Note that 5000 nodes correspond to only ~ 17 points per coordinate, with the average separation distance of $h \approx L_{\text{dom}}/17 \approx 0.59$, which is comparable with the radius of the particle. Clearly, classical FD schemes would require much finer meshes for high accuracy (and still would not be able to deliver machine precision).

Let us now return to the test problem with *two particles*, as described above. Fig. 11 presents the general setup of the problem solved with a random distribution of 8000 nodes (only 1600 shown in the picture); the simulation results are reported below. Fig. 12 shows projections of the same nodes and of the spheres on the xy -plane.

Table 3 shows the dependence of the numerical error on the number of random nodes. The errors are still quite small despite the highly suboptimal distribution of nodes. At the same time, as could be expected, the errors are higher than for regular grids and, moreover, convergence of the solution with respect to the number of nodes is not monotone. This is almost certainly attributable to “poor quality” stencils, although precise *a priori* measures of quality in FLAME are still to be developed; see further comments on that below.

One may envision that in future applications of the new version of FLAME the nodal distributions will be optimized and generated adaptively, based on appropriate *a posteriori* error estimates. Such distributions can then be expected to produce more accurate solutions than random, semi-random or even regular sets of nodes would.

A natural *a posteriori* error indicator⁶ in FLAME is the discrepancy between the values of the solution over two overlapping patches; this indi-

⁶ As in FEM, one may want to distinguish *estimators* that produce some quantitative measure of the error from qualitative *indicators* of regions where grid refinement is desirable.

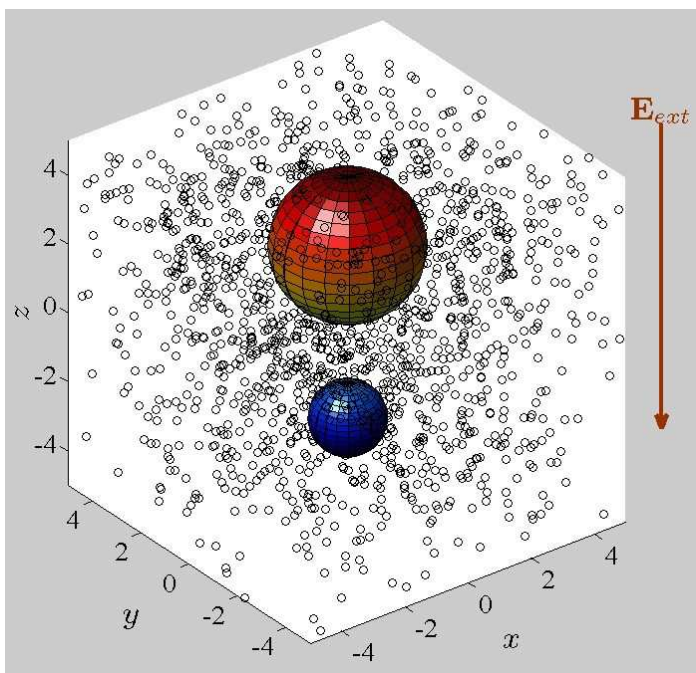


Fig. 11 Two dielectric spheres in an external field. An example of least squares FLAME with 8,000 randomly generated nodes (only 1,600 shown for visual clarity). Nodes inside the particle not visible but are distributed with the same density.

Number of nodes	Effective “grid size”	Relative error
10000	0.464	1.94E-04
20000	0.368	3.66E-04
30000	0.322	2.76E-05
40000	0.292	3.16E-05
60000	0.255	2.11E-05

Table 3 Relative errors in the nodal potential for FLAME on *fully random* sets of nodes. The reference quasi-analytical solution is obtained by the multipole-multicenter (mmc) expansion with 64 terms per particle. 3D test problem with two dielectric particles with the dielectric permittivity 5. 19-point stencils with 9 basis functions.

cator has already been shown to produce quite reasonable results, leading to grid refinement around the gaps between two neighboring particles [8, 47]. It should certainly be possible to develop other, and better, indicators in the future.

Likewise – and also in parallel with FEM where similar issues have been studied for several decades – good *a priori* error estimates indicating the “quality” of irregular stencils are needed. In FEM, there are several geometric conditions that characterize the quality of elements (“quality” being

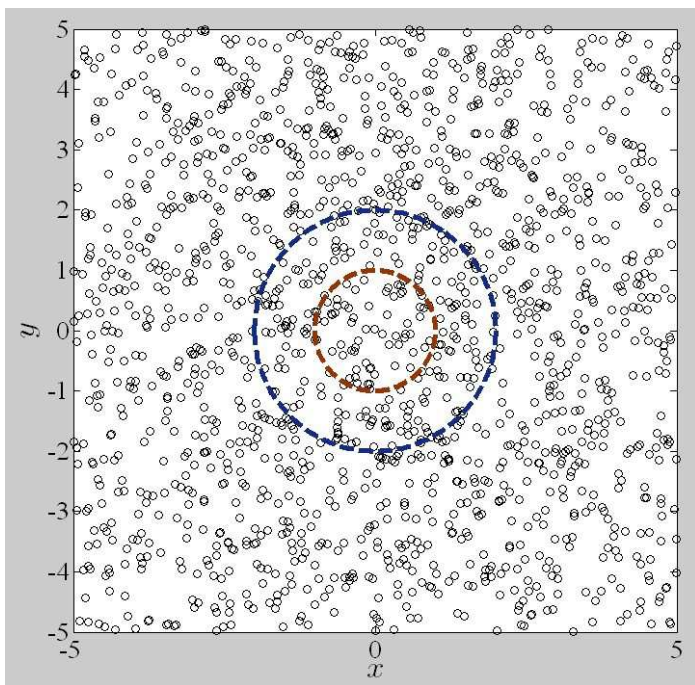


Fig. 12 Same as in the previous figure, but projections of the nodes and of the two particles on the xy -plane shown. Note that the exterior Dirichlet boundary in this example is “fuzzy”.

ultimately understood as approximation accuracy): for example, the minimum or maximum angle conditions, the radius of the inscribed sphere vs. the element diameter, etc.

In comparison with FEM, irregular stencils (especially large ones) are difficult to characterize in pure geometric terms. Therefore particularly relevant are the *algebraic* conditions. In FEM, such conditions are related to the properties of the affine transformation of a given element to the canonical “master” element [48, 49] or, in less traditional analysis (see [2], §3.14), to the maximum eigenvalue of the element stiffness matrix or the minimum singular value of the edge shape matrix [52, 53, 51, 50]. One conjecture that may form an interesting subject for future research is that for least squares FLAME the minimum singular value of the nodal matrices such as N (4) will play a similar role.

8 Conclusion

FLAME replaces standard Taylor expansions of classical finite difference methods with local approximations of the solution by functions satisfying the underlying differential equation and interface boundary conditions. As

a result, it is not unusual for the consistency error of FLAME to be orders of magnitude lower than that of conventional schemes, due to the high accuracy of the Trefftz approximations employed in FLAME.

Previously one constraint in FLAME has been that the number of approximating functions had to be closely linked to the number of nodes in the grid stencil. The present paper, by expanding on the idea of Pinheiro & Webb [9], removes this constraint: while Trefftz functions still provide very accurate approximation, the numbers of functions and nodes are now decoupled. This is accomplished by using least-squares matching of the approximate solution at the stencil nodes. Consequently, FLAME schemes can now be generated on irregular stencils with the number of nodes substantially greater than the number of approximating functions. This extends the practical applicability of the method.

Counterintuitively, the use of the least squares fit instead of the exact nodal match does not reduce the numerical accuracy; on the contrary, the method tends to become more robust. The consistency error is still governed primarily by the approximation accuracy of the solution with the Trefftz-FLAME basis.

In contrast with meshless methods and other similar techniques, the treatment of interface and exterior boundary conditions in FLAME is simple and natural. Trefftz-FLAME basis functions satisfy the underlying equation and the boundary conditions by construction and therefore do not require any additional constraints to be imposed.

In summary, the new version of FLAME is a promising technique that combines the high accuracy of Trefftz approximations with robust operation on irregular stencils. Once a set of basis functions is established, FLAME is exceptionally easy to implement in computer codes, as it does not require mesh generation, numerical integration or differentiation. The ability of the method to handle irregular stencils, as well as the *a posteriori* error indicators inherent in FLAME, bodes well for the development of adaptive algorithms in the future.

The price to pay for these advantages is the need to derive the local Trefftz sets. Expanding the library of canonical solutions (e.g. elliptic problems / wave scattering; (piecewise) planar / cylindrical / spherical boundaries, etc.) may lead to the commensurate expansion of the applicability of FLAME. On the other hand, problems where local solutions are unavailable or difficult to obtain may remain out of reach for FLAME until additional ideas are put forward.

An interesting subject for future research is *a priori* and *a posteriori* error estimates in FLAME. Some considerations are already presented in this paper.

In comparison with the previous version of Trefftz-FLAME, least squares FLAME is particularly promising in cases where an intrinsic disparity between the natural sizes of the bases and stencils exists. Examples include finite difference time domain simulation of wave propagation, as well as

electromagnetic vector problems where this version of FLAME has already been explored [9].

References

1. Igor Tsukerman, A class of difference schemes with flexible local approximation. *J. of Comp. Phys.* 211 (2) (2006) 659–699.
2. Igor Tsukerman, *Computational Methods for Nanoscale Applications: Particles, Plasmons and Waves*, Springer ©2008.
3. V. M. A. Leitão, Generalized finite differences using fundamental solutions, *Int J for Numer Meth Eng*, (2009) doi: 10.1002/nme.2697 (to appear).
4. Igor Tsukerman, Electromagnetic applications of a new finite-difference calculus. *IEEE Trans. Magn.* 41 (7) (2005) 2206–2225.
5. Igor Tsukerman and František Čajko, Photonic band structure computation using FLAME, *IEEE Trans. Magn.*, 44 (6) (2008) 1382–1385.
6. J. Dai, I. Tsukerman, A. Rubinstein, S. Sherman. New computational models for electrostatics of macromolecules in solvents. *IEEE Trans. Magn.* 43 (4) (2007) 1217–1220.
7. Igor Tsukerman. Quasi-homogeneous backward-wave plasmonic structures: Theory and accurate simulation. *J. Opt. A: Pure Appl. Opt.* 11 (2009) 114025.
8. Jianhua Dai, Igor Tsukerman, Flexible approximation schemes with adaptive grid refinement, *IEEE Trans. Magn.* 44(6) (2008) 1206–1209.
9. H. Pinheiro, J.P. Webb. A FLAME Molecule for 3-D electromagnetic scattering. *IEEE Trans. Magn.* 45 (3) (2009) 1120–1123.
10. V Nguyen, T Rabczuk, S Bordas, M Duflot. Meshless methods: A review and computer implementation aspects. *Mathematics and Computers in Simulation* 79 (3) (2008) 763–813.
11. Belytschko T, Lu YY, Gu L. Element-free Galerkin methods. *Int. J. for Num. Meth. in Eng.* 37 (2) (1994) 229–256.
12. Belytschko T, Krongauz Y, Organ D, Fleming M, Krysl P. Meshless methods: An overview and recent developments. *Computer Methods in Appl Mech and Eng.* 139 (1-4) (1996) 3–47.
13. Krongauz Y, Belytschko T. EFG approximation with discontinuous derivatives. *Int J for Num Meth in Eng* 41 (7) (1998) 1215–1233.
14. W. Liu, S. Jun, Y. Zhang, Reproducing kernel particle methods, *Int. J. Numer. Meth. Fluids* 20 (1995) 1081–1106.
15. Ivo Babuška, Uday Banerjee, John E. Osborn, Survey of meshless and generalized finite element methods: a unified approach. *Acta Numer.* 12 (2003) 1–125.
16. N. Sukumar. Construction of polygonal interpolants: A maximum entropy approach. *Int J for Num Meth in Eng* 61 (12) (2004) 2159–2181.
17. M. Arroyo and M. Ortiz. Local maximum-entropy approximation schemes: a seamless bridge between finite elements and meshfree methods. *Int J for Num Meth in Eng* 65 (2006) 2167–2202.
18. Shari Moskow, Vladimir Druskin, Tarek Habashy, Ping Lee and Sofia Davydcheva. A finite difference scheme for elliptic equations with rough coefficients using a Cartesian grid nonconforming to interfaces. *SIAM J on Num Analysis* 36 (2) (1999) 442–464.
19. Isaac Harari. A survey of finite element methods for time-harmonic acoustics *Comput. Methods Appl. Mech. Engrg.* 195 (2006) 1594–1607.

20. Larry A. Lambe, Richard Luczak, John W. Nehrass. A New Finite Difference Method For The Helmholtz Equation Using Symbolic Computation. *Int J of Comput Eng Sci* 4(1) (2003) 121–144.
21. I. Singer and E. Turkel. Sixth-order accurate finite difference schemes for the Helmholtz equation. *J of Comput Acoustics* 14 (3) (2006) 339–351.
22. Guy Baruch, Gadi Fibich, Semyon Tsynkov and Eli Turkel Fourth order schemes for time-harmonic wave equations with discontinuous coefficients. *Commun. Comput. Phys.* 5 (2009) 442–455.
23. Majid Nabavi, M.H. Kamran Siddiqui and Javad Dargahia. A new 9-point sixth-order accurate compact finite-difference method for the Helmholtz equation. *Journal of Sound and Vibration* 307(3–5) (2007) 972–982.
24. Godehard Sutmann. Compact finite difference schemes of sixth order for the Helmholtz equation. *J of Comput and Appl Math.* 203 (1) (2007) 15–31.
25. K.K. Mei, R. Pous, Z. Chen, Y.W. Liu, M.D. Prouty. Measured equation of invariance: a new concept in field computation, *IEEE Trans. Antennas Propagation* 42 (1994) 320–327.
26. R. Mittra and O. M. Ramahi. Absorbing boundary conditions for direct solution of partial differential equations arising in electromagnetic scattering problems. In: J. A. Kong and M. A. Morgan (Eds.) *Differential Methods in Electromagnetic Scattering*, Elsevier, 1989, pp. 133–173 Chap. 4.
27. A. Boag and R. Mittra. A numerical absorbing boundary condition for finite difference and finite element analysis of open periodic structures. *IEEE Trans. Microwave Theory Tech.* 43 (1995) 150–154.
28. A. Boag, A. Boag, R. Mittra, and Y. Leviatan, A numerical absorbing boundary condition for finite difference and finite element analysis of open structures. *Microwave and Optical Tech Lett* 7 (1994) 395–398.
29. G. Ronald Hadley. High-accuracy finite-difference equations for dielectric waveguide analysis I: uniform regions and dielectric interfaces. *Journal of Lightwave Technology*, 20(7) (2002) 1210–1218.
30. G. Ronald Hadley. High-accuracy finite-difference equations for dielectric waveguide analysis II: dielectric corners. *Journal of Lightwave Technology*, 20(7) (2002) 1219–1231.
31. Y.-C. Chiang, Y.-P. Chiou, and H.-C. Chang, Finite-difference frequency-domain analysis of 2-D photonic crystals with curved dielectric interfaces, *J. Lightw. Technol.* 26 (2008) 971–976.
32. Yen-Chung Chiang, Higher order finite-difference frequency domain analysis of 2-D photonic crystals with curved dielectric interfaces. *Optics Express* 17 (5) (2009) 3305–3315.
33. Yuan J and Lu Y. Photonic bandgap calculations with Dirichlet-to-Neumann maps *J. Opt. Soc. Am. A* 23 (2006) 3217–3222.
34. Hu Z and Lu Y Y Efficient analysis of photonic crystal devices by Dirichlet-to-Neumann maps. *Opt. Express* 16 (2008) 17383–17399.
35. Roger F. Harrington, *Time-Harmonic Electromagnetic Fields*, Wiley-IEEE Press, 2001.
36. František Čajko and Igor Tsukerman, Flexible approximation schemes for wave refraction in negative index materials. *IEEE Trans. Magn.* 44 (6) (2008) 1378–1381.
37. V.P. Bykov. Spontaneous emission in a periodic structure. *Soviet physics, JETP (Journal of Experimental and Theoretical Physics)*, 35(2) (1972) 269–273.

38. V.P. Bykov. Spontaneous emission from a medium with a band spectrum. *Sov. J. Quant. Electron.* 4(7) (1975) 861–871.
39. Eli Yablonovitch. Inhibited spontaneous emission in solid-state physics and electronics. *Phys. Rev. Lett.* 58(20) (1987) 2059–2062.
40. Sajeev John. Strong localization of photons in certain disordered dielectric superlattices. *Phys. Rev. Lett.* 58(23) (1987) 2486–2489.
41. Steven G. Johnson and J.D. Joannopoulos, Block-iterative frequency-domain methods for Maxwell’s equations in a planewave basis, *Opt. Express*, Vol. 8, No. 3, pp. 173–190, 2001.
42. Kazuaki Sakoda. *Optical Properties of Photonic Crystals*, Berlin; New York: Springer, 2005.
43. Takeshi Fujisawa and Masanori Koshiba. Time-domain beam propagation method for nonlinear optical propagation analysis and its application to photonic crystal circuits. *J. of Lightwave Technology*, 22(2) (2004) 684–691.
44. H. Pinheiro, J.P. Webb, I. Tsukerman. Flexible local approximation models for wave scattering in photonic crystal devices. *IEEE Trans. Magn.* 43 (4) (2007) 1321–1324.
45. H. Cheng, L. Greengard, and V. Rokhlin. A fast adaptive multipole algorithm in three dimensions. *J. Comp. Phys.* 155 (2) (1999) 468–498.
46. M.I. Mishchenko, L.D. Travis, and A.A. Lacis. *Scattering, Absorption, and Emission of Light by Small Particles*. Cambridge University Press, 2002.
47. Jianhua Dai, Helder Pinheiro, J.P. Webb, Igor Tsukerman, Flexible approximation schemes with numerical and semi-analytical bases, submitted.
48. N. Al Shenk, Uniform error estimates for certain narrow lagrange finite elements. *Math. of Comp.* 63 (1994) 105–119.
49. P.G. Ciarlet, *The Finite Element Method for Elliptic Problems*, North-Holland: Amsterdam, 1978.
50. Igor Tsukerman and Alexander Plaks. Refinement strategies and approximation errors for tetrahedral elements. *IEEE Trans. Magn.* 35 (3) (1999) 1342–1345.
51. Igor Tsukerman, Alexander Plaks. Comparison of accuracy criteria for approximation of conservative fields on tetrahedra. *IEEE Trans. Magn.* 34 (1998) 3252–3255.
52. Igor Tsukerman. A general accuracy criterion for finite element approximation. *IEEE Trans. Magn.* 34 (1998) 2425–2428.
53. Igor Tsukerman, Approximation of conservative fields and the element “edge shape matrix”. *IEEE Trans. Magn.* 34 (1998) 3248–3251.